CORROSION AND CORROSION FATIGUE OF AIRFRAME ALUMINUM ALLOYS

G. S. Chen, M. Gao, D. G. Harlow and R. P. Wei
Mechanical Engineering and Mechanics
LEHIGH UNIVERSITY
Bethlehem, PA 18015 USA

ABSTRACT

Localized corrosion and corrosion fatigue crack nucleation and growth are recognized as degradation mechanisms that affect the durability and integrity of commercial transport aircraft. Mechanistically based understanding is needed to aid the development of effective methodologies for assessing durability and integrity of airframe components. As a part of the methodology development, experiments on pitting corrosion, and on corrosion fatigue crack nucleation and early growth from these pits were conducted. Pitting was found to be associated with constituent particles in the alloys and pit growth often involved coalescence of individual particle-nucleated pits, both laterally and in depth. Fatigue cracks typically nucleated from one of the larger pits that formed by a cluster of particles. The size of pit at which fatigue crack nucleates is a function of stress level and fatigue loading frequency. The experimental results will be summarized, and their implications on service performance and life prediction will be discussed.

INTRODUCTION

Localized corrosion (in the form of pitting and exfoliation in aluminum alloys), and corrosion fatigue crack nucleation and growth are clearly recognized as degradation mechanisms that affect the durability and integrity of commercial transport aircraft. A quantitative methodology for establishing suitable intervals for inspection and repair, and for assessing the durability and integrity of airframe components, is needed for the effective management of the nation's aging fleet of commercial transport aircraft. The development of such a methodology requires a quantitative understanding, characterization and modeling of the elemental processes of damage, and the integration of the various models into a suitable probabilistic framework for service life prediction. Such an understanding of the damaging mechanisms and the formulation of a predictive methodology will also assist in the design of new aircraft and in the development of suitable "fixes" for the current fleet.

In this paper, a summary of progress is presented for the areas of localized corrosion and corrosion fatigue crack nucleation of an FAA sponsored program on airframe materials. This 3-year program of research is directed at studies of corrosion and corrosion fatigue of airframe materials in support of the FAA Aging Airplanes Program, and was initiated on 15 June 1992. The experimental portion of the program is focused on 2024-T3 (bare) aluminum alloy sheet material.

OBJECTIVES AND SCOPE

The objectives of the program are: (1) to develop basic understanding of the processes of localized corrosion and corrosion fatigue crack nucleation and growth in high strength aluminum alloys used in airframe construction, (2) to develop kinetic models for these elemental processes, and (3) to integrate these models into probabilistic models that can provide guidance in formulating methodologies for service life prediction.

The development of damage is illustrated schematically in Fig. 1, and is shown in a flow diagram in Fig. 2a. The early stage is dominated by corrosion, in the form of pitting or exfoliation, and the later stage by corrosion fatigue crack growth. Within the context of these mechanisms, an upper bound of damage is to be defined in terms of structural reliability and damage tolerance considerations regarding repairs. The research is focused, therefore, on the quantitative understanding and characterization, and kinetic modeling, of the following elemental processes:

- Onset of localized corrosion damage (particularly, mechanisms and kinetics of corrosion pit nucleation and growth).
- Transition from pitting to fatigue crack growth (or crack nucleation).
- Early stages of corrosion fatigue crack growth (short-crack regime).
- Corrosion fatigue crack growth.

Formulation of a predictive model would have to include the probabilistic contributions from material properties and key variables on the rate of corrosion (particularly, pit nucleation and growth, and exfoliation) and corrosion fatigue crack growth, and on the transition from corrosion to cracking.

The following principal issues are being addressed, and the overall modeling framework is shown by the block diagram in Fig. 2b.

- Identification and verification of key internal and external variables that control each of the aforementioned unit processes for corrosion and corrosion fatigue cracking and determination of the stochastic nature of each process
- Quantification of the probability distribution function (including time variance) of each of the key variables
- Development of quantitative understanding of the rate controlling step and mechanism for each damage process, and formulation of a mechanistic (*deterministic*) model for each that describes the functional dependence on the key variables
- Integration of mechanistic models and probability distribution functions, and formulation of mechanistically based probability models for life prediction and reliability assessment

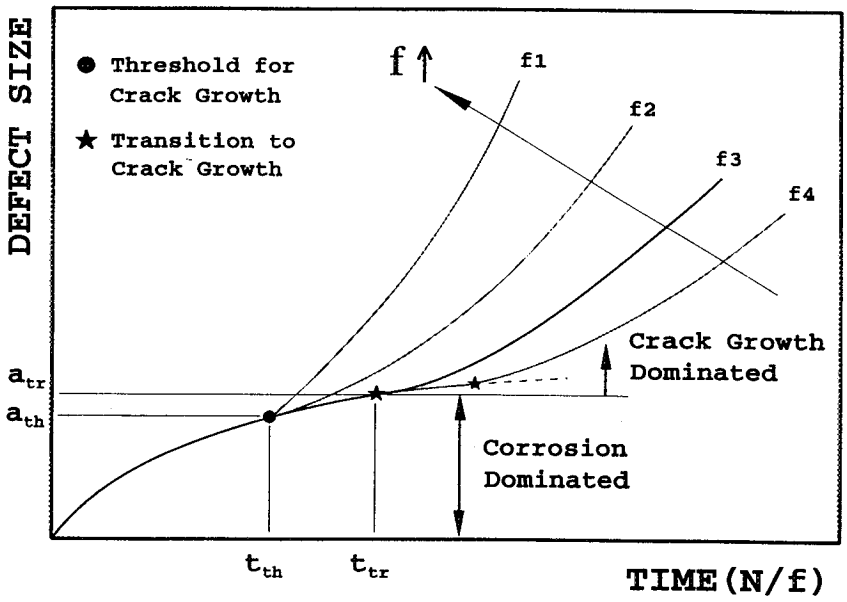

Figure 1. Schematic representation of localized corrosion (pitting or exfoliation) and corrosion fatigue.

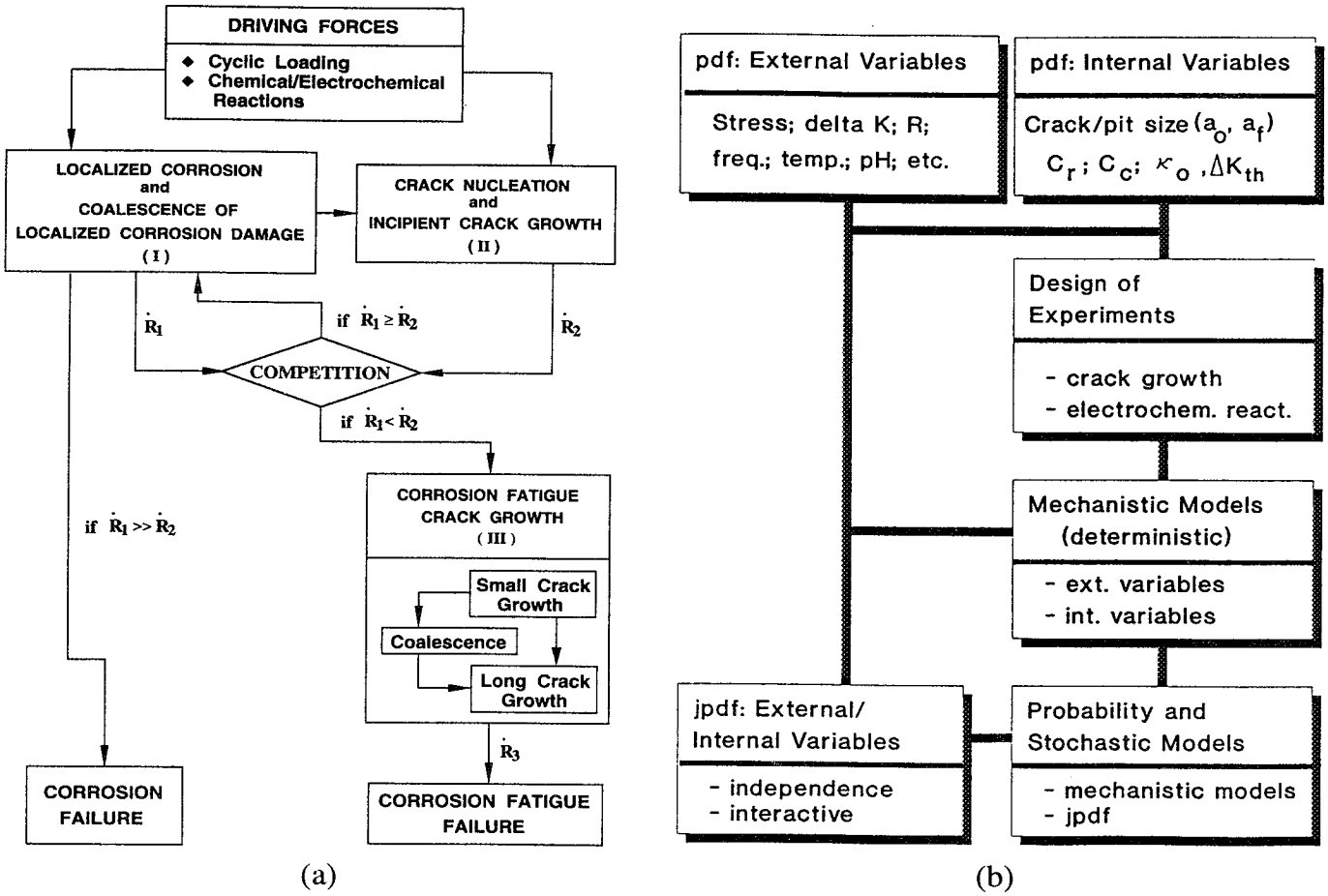

Figure 2. (a) Flow diagram showing the overall processes for corrosion and fatigue damage, and (b) key elements for the formulation of a mechanistically based probability model for life prediction.

The results described herein are restricted to the pitting and crack nucleation (transition) processes. The environment and experimental conditions used (for example, continuous full immersion in an aqueous solution) tend to accelerate damage accumulation. As such, these results should not be applied directly in assessing material performance in service.

PITTING CORROSION

A 1.6 mm (0.06 in.) thick sheet of bare 2024-T3 aluminum alloy is used in this study. The chemical composition is given in Table I, and its microstructure is shown in Fig. 3. Both standard polished and etched sections and back-scattered electron SEM micrographs of un-etched sections are included to show the microstructure and the size and distribution of constituent particles.

Table I. Chemical Composition (wt%) of the 2024-T3 Alloy

Component	Al	Cu	Mg	Mn	Fe	Si	Ti	Cr	Zn
Nominal*	Balance	3.8-4.9	1.2-1.8	0.3-0.9	0.50	0.50	0.15	0.10	0.25
Measured**	93.52	4.24	1.26	0.65	0.15	0.06	0.031	<0.01	0.08

* Metal Handbook, 9th ed., vol. 2, ASM International, Metals Park, OH, 1990, p. 17.
** Laboratory Testing Inc., Dublin, PA.

The as-received material was cut into 10mm x 10mm specimens for corrosion testing. The specimens were ground through a graded series of SiC papers, and then polished with diamond paste and colloidal SiO_2 to achieve mirror-like flat surfaces (~0.05μm rms surface roughness). After polish-ing, the specimens were cleaned with water and ethyl alcohol, and dried with warm air. Prior to corrosion testing, each specimen was coated with stop-off lacquer so that only the polished surface would be exposed to the test environment. For these studies, 0.5M NaCl (sodium chloride) solution was used. The solution was prepared by mixing reagent grade sodium chloride crystals with de-ionized water. The corrosion experiment was performed by simply immersing the specimen in a covered glass jar containing 200 mℓ of 0.5M NaCl solution, under free corrosion condition and without mechanical disturbance, principally at room temperature (~23°C) for specific periods of time. Some tests were carried out at 5°, 40°, 65° and 80°C. Before corrosion testing, the solution pH was typically about 5.8 (5.5 to 6) and the oxygen concentration, approximately 7 ppm. A few tests were also conducted at pH of 3 and 11. The solution pH and oxygen level were not controlled during the course of these corrosion tests. After testing for 24 hours at 80°C, for example, the pH increased slightly to 6.7 from 5.8 and the oxygen level dropped to 5.2 from 6.6 ppm.

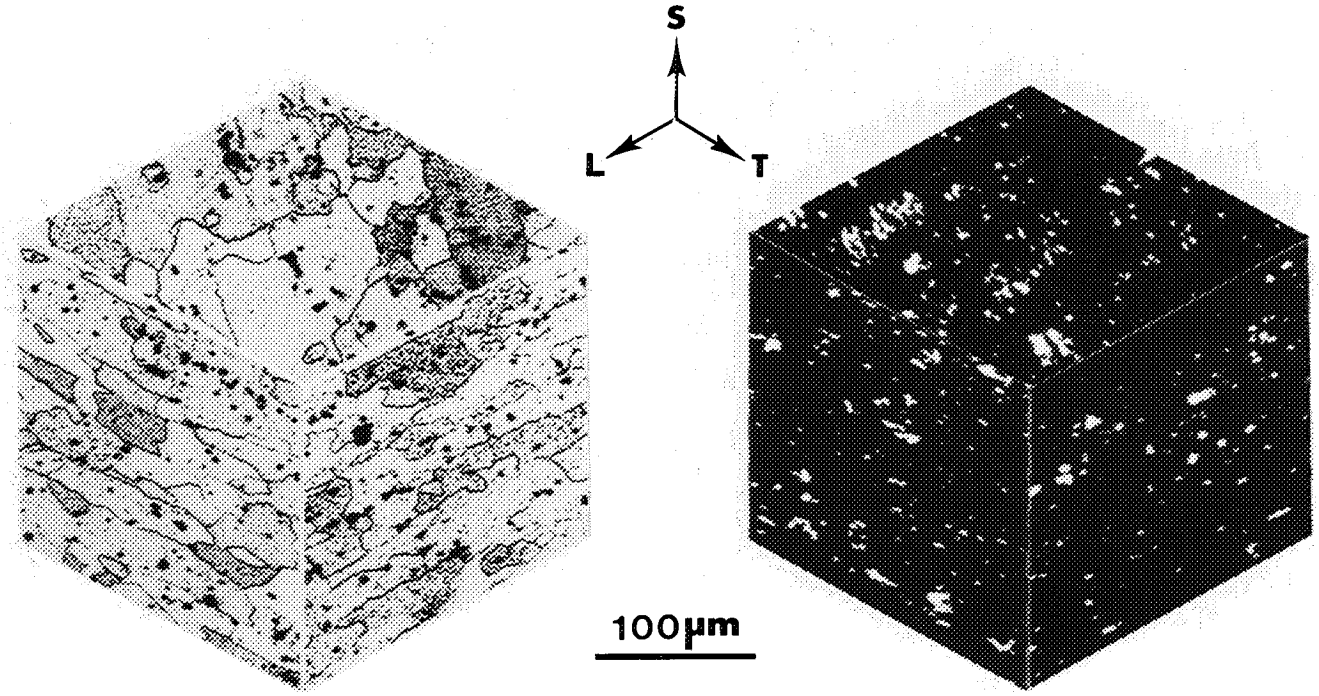

(a) (b)

Figure 3. (a) Metallographic features in bright field optical image showing the microstructure of the 2024-T3 aluminum alloy, and (b) constituent particles in SEM backscattered electron contrast showing the particle morphology and distribution.

After corrosion testing, the specimens were washed with deionized water, acetone and ethanol, and dried with warm air. In some cases, a solution containing phosphoric acid (H_3PO_4) and chromic trioxide (Cr_2O_3) was used to remove oxides and corrosion products from the specimen surface. Optical and scanning electron microscopy (OM and SEM) and energy dispersive x-ray spectroscopy (EDX) were then used to investigate the surface morphology and chemical composition of the alloy surface and constituent particles.

Role of Constituent Particles

Figure 4 shows optical micrographs of the same (representative) area of a polished, bare 2024-T3 aluminum alloy surface before and after corrosion. The presence of a large number of constituent particles is evident. It is also clear that early corrosion is associated with these constituent particles. Some clustering of the particles is evident, and there is some banding of particles along the rolling direction of the sheet. The average density of particles with a projected surface area greater than one square micrometer (*i.e.*, >1 μm^2) was found to be about 3,230 particles per square millimeter, and the surface areal fraction of the particles was estimated to be about 2.7 percent. Typical size distribution for these particles is shown in Fig. 5 in a Weibull format [1].

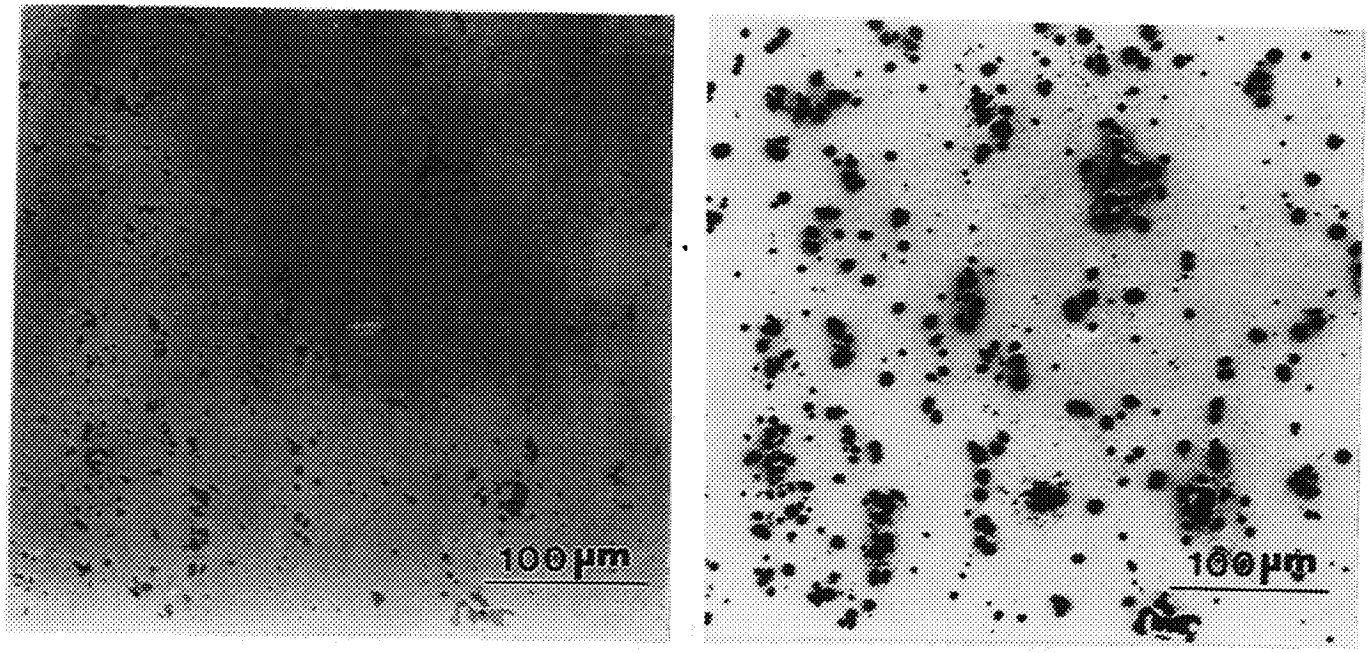

(a) (b)

Figure 4. Optical micrographs for the same area of a bare 2024-T3 aluminum specimen showing (a) an as-polished surface, and (b) a corroded surface after 3-hours in 0.5M NaCl solution (pH ≈ 5.8) at room temperature.

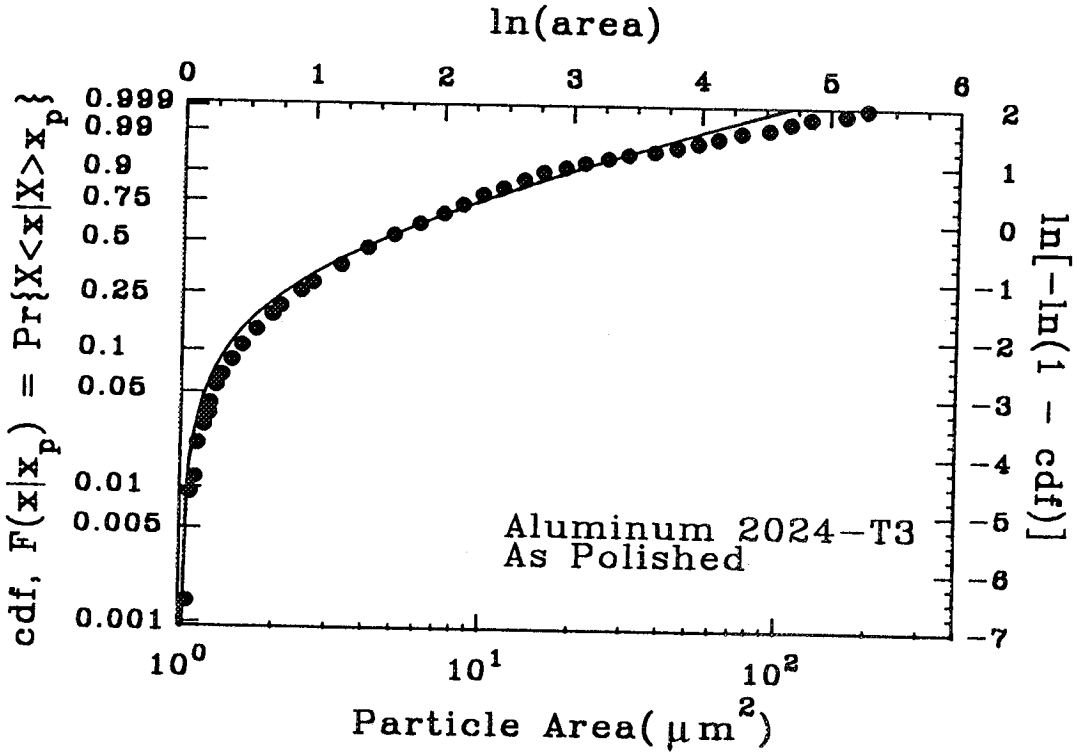

Figure 5. Typical size distribution in a Weibull format for the constituent particles in the 2024-T3 aluminum alloy.

The morphology, chemical composition and corrosion behavior of the particles were examined by SEM and EDX, and typical results are shown in Table II and in Figs 6 and 7. Two types of constituent particles with differing corrosion behavior may be seen from EDX results on selected particles before and after corrosion testing at 80°C, Table II; namely, those that contain only Al, Cu and Mg, before corrosion; and those that contain Al, Cu, Fe and Mn, with no Mg. The distribution and relative concentration of these particles are shown by a comparison of the SEM micrograph and corresponding elemental maps of a typical region, for example, in Fig. 6. Some clustering and mingling of the two types of particles are seen. The fraction of Al-Cu-Mg particles (those not containing Fe in Fig 6) was estimated to be about 75 percent in this alloy.

Table II. Comparison of EDX Results for Individual Particles *Before* and *After* Corrosion in 0.5M NaCl Solution at 80°C for 24 Hours

Particle Type	Corrosion Testing	$K\alpha$ Intensity (counts)				
		Mg	Mn	Fe	Cu	Al
A1	before	678	ND*	ND	9600	2990
	after	ND	ND	495	11362	474
A2	before	804	ND	ND	7086	3516
	after	ND	523	640	5710	1892
A3	before	1437	ND	ND	6593	8411
	after	ND	468	534	6354	840
A4	before	2209	ND	ND	2798	11024
	after	ND	681	619	5061	4671
C1	before	ND	3485	4644	4379	1057
	after	ND	433	1092	9666	4671
C2	before	ND	2132	2972	5541	2086
	after	ND	702	3078	7843	700
C3	before	ND	3280	3960	4067	5057
	after	ND	968	5072	3359	1337
C4	before	ND	2723	3438	4725	5997
	after	ND	689	4997	2443	1470

* ND: not detected.

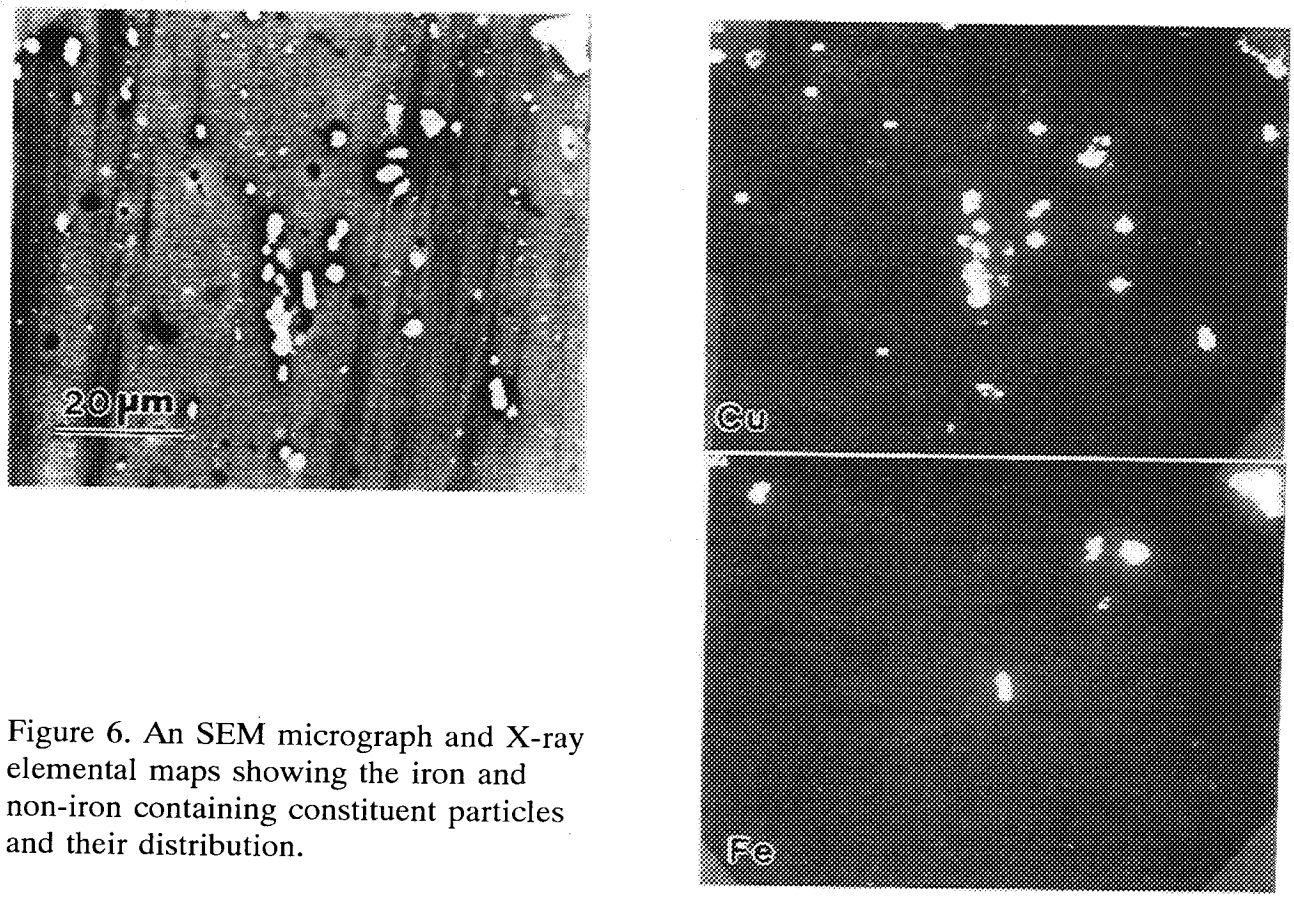

Figure 6. An SEM micrograph and X-ray elemental maps showing the iron and non-iron containing constituent particles and their distribution.

From a comparison of the EDX results in Table II, it is clear that the Mg in all of the Al-Cu-Mg particles was removed by corrosion. Further mechanistic interpretation of these EDX data, however, would require more detailed analyses. Nevertheless, some insight may be gained through a comparison with SEM and EDX analyses of individual particles after corrosion (see Fig. 7). It may be seen that the Al, Cu, Mn and Fe containing particles (*e.g.*, particle at C in Fig. 7a and the corresponding EDX spectra in Fig. 7b) promoted matrix dissolution at their periphery. Those particles that contain Al, Cu and Mg, on the other hand, dissolved (*e.g.*, particles at A in Fig. 7a and the associated spectra in Fig. 7b), and had mostly Cu left. The P and Cr peaks in the EDX spectra (Fig. 7b) are principally residues from chemical cleaning.

The Al-Cu-Mg-containing particles, therefore, acted as anodic sites and lost Mg and Al through dissolution (or dealloying) in the early stage of corrosion, but became more cathodic as copper was left behind (see Table II and particle A in Fig. 7). Dealloying of an intermetallic T_1 phase (Al_2CuLi) and dealuminization of γ_2 (Cu_2Al) compounds have been reported in the literature [2,3]. There is evidence of Fe and Mn deposition onto the Al-Cu-Mg particle sites (though not seen in Fig. 7) during corrosion. On the other hand, copper deposition was observed on the Al-Cu-Mn-Fe containing particles, with nodular copper deposits on these particles irrespective of their size (as indicated by the arrows in Fig. 7a). The phenomenon is similar to that of deposition corrosion [4,5]. This behavior suggests that the Al-Cu-Mn-Fe containing particles served as cathodic sites in the corrosion process, and led to the reduction of cupric ions dissolved in the solution. The data on Fe and Mn (Table II) are less clear because of Cu deposition on some of the particles. The SEM evidence (Fig. 7) suggests that these particles promoted dissolution of the adjacent matrix, but, by and

large, did not dissolve themselves. It is to be noted that no evidence of exfoliation was uncovered in this study.

The form of localized corrosion (i.e. particle-induced pitting) was not altered by temperature, but the degree and rate of pitting damage was enhanced with increasing solution temperature. Particle-induced pitting corrosion was found to be less severe in an acidic (pH = 3) solution, probably because of enhanced general corrosion, and in an alkaline (pH =11) solution, because of reduced passive film integrity attenuating localized attack.

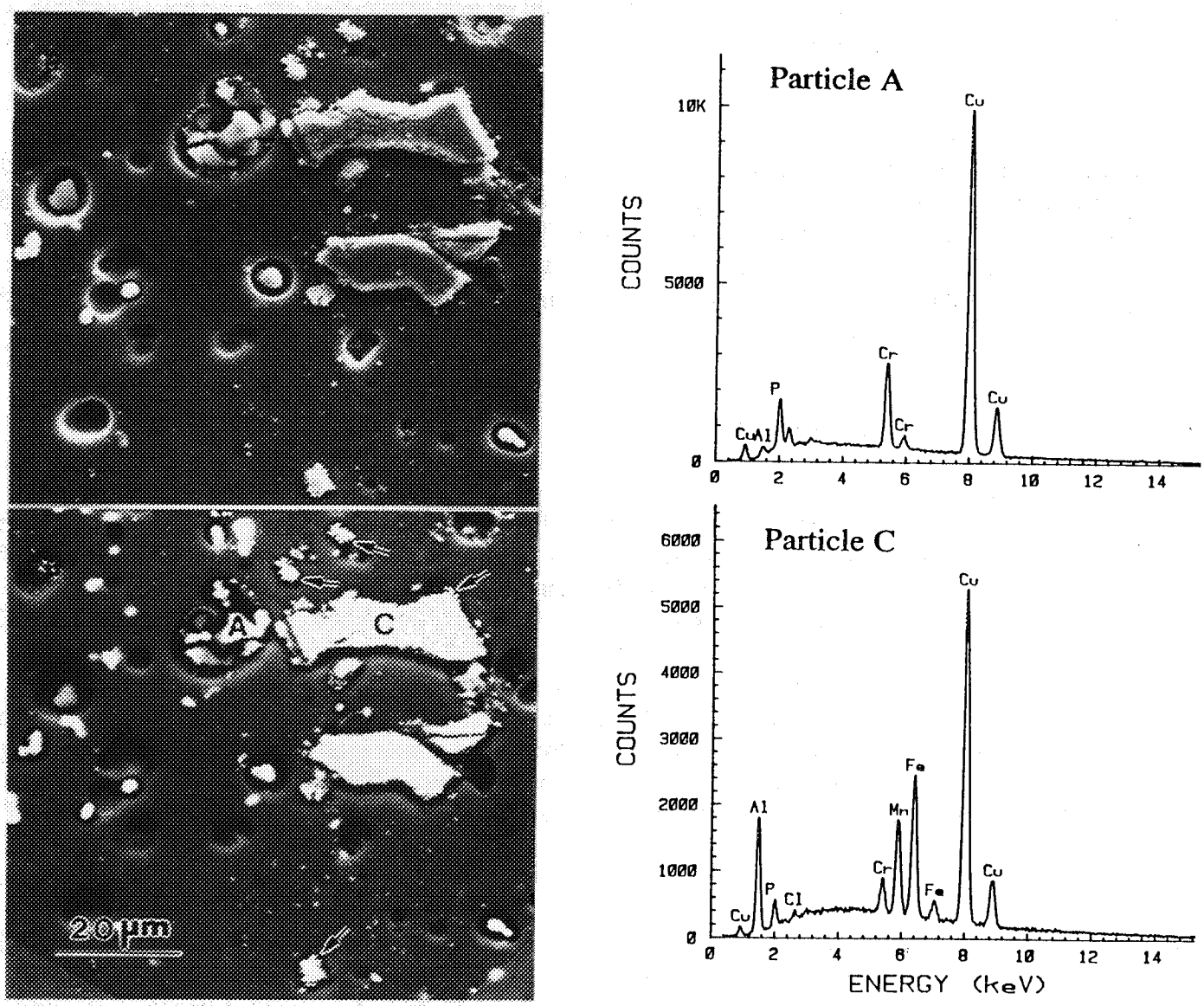

(a) (b)

Figure 7. SEM and EDX results for a bare 2024-T3 aluminum alloy specimen tested in 0.5M NaCl solution (pH ≈ 5.8) at room temperature for 3 days, showing (a) localized corrosion at constituent particles (top: secondary electron contrast; bottom: backscattered electron contrast), and (b) chemical composition of the particles at A and C in the micrograph. (Arrows point to copper deposition on the Al-Cu-Mn-Fe particles.)

Growth and Coalescence, and Orientation Dependence

The evolution of pitting damage may be seen from a representative SEM micrograph and a Gumbel plot [6] of distributions in pit size at 40°C, Figs 8a and 8b. The results for longer periods of time (*e.g.*, three days or 72 hours, Fig. 8a) confirm the identification of constituent particles as the primary sites for pitting corrosion. Taken together with Fig. 8b, the results provide an indication of the evolution of particle-nucleated pitting damage in the 2024-T3 aluminum alloy. The individual pits grew both in breadth and in depth with time, and can coalesce to form a larger pit (in Fig. 8a). Accelerated pitting may result from this process of pit coalescence rather than through single pit growth.

The process is very complex and appears to involve 3-D interactions with constituent particles. Corrosion sensitivity appears to be orientation dependent, being *more severe in the thickness orientation* because of local segregation of constituent particles. Such enhanced pitting at the surface of a drilled and polished hole is shown in Fig. 9, and fatigue cracks have been observed to nucleate from such pits. It is interesting to note that severe corrosion (anodic dissolution) at the large active pit appears to cathodically protect the neighboring surface, resulting in lightly corroded "plateaus" over the surface.

TRANSITION FROM PITTING TO FATIGUE CRACK GROWTH

Corrosion fatigue failures often result from the nucleation and growth of fatigue cracks from corrosion induced pits [7,8]. Cracking occurs when the local mechanical condition is adequate for the onset of crack growth. Recently, Kondo [9] and Kondo and Wei [10] considered the competition between corrosion pit and fatigue crack growth in steels, and proposed a criterion for the transition from pitting to corrosion fatigue crack growth, Fig. 1. The criterion is based on the assumption that a corrosion pit may be modeled by an equivalent semi-elliptical (or semi-circular) surface crack. It suggests that transition from pit growth to fatigue crack growth takes place when the stress intensity factor of the equivalent surface crack reaches the threshold stress intensity factor (ΔK_{th}) for fatigue crack growth. Through this criterion a linkage is made between the critical pit size (for a given applied stress) and a fracture mechanics parameter to provide a framework for the prediction of pitting/corrosion fatigue life.

Fatigue experiments were carried out on open-hole specimens of 2024-T3 (bare) alloy in 0.5M NaCl solution at room temperature and different loading frequencies from 0.1 to 10 Hz. The maximum stress applied at the hole was estimated to be 320 MPa and the load ratio, R, was 0.1. Cracks were found to nucleate from areas of severe local corrosion; namely, *pits* (Figs 10a and 10b). Fatigue failure, by-and-large, resulted from a *single* nucleation site, although many secondary cracks were observed to form at corrosion pits away from the main fatigue crack (Fig. 11). Hence, a dominant flaw model for corrosion and corrosion fatigue appears to be appropriate.

In contradistinction to the original concept of Kondo [9] and Kondo and Wei [10], the pit-to-crack transition size (or crack nucleation size) appears to depend on the cyclic-load frequency being larger at lower frequencies (see Figs 10a and 10b, and Table III). This frequency dependence

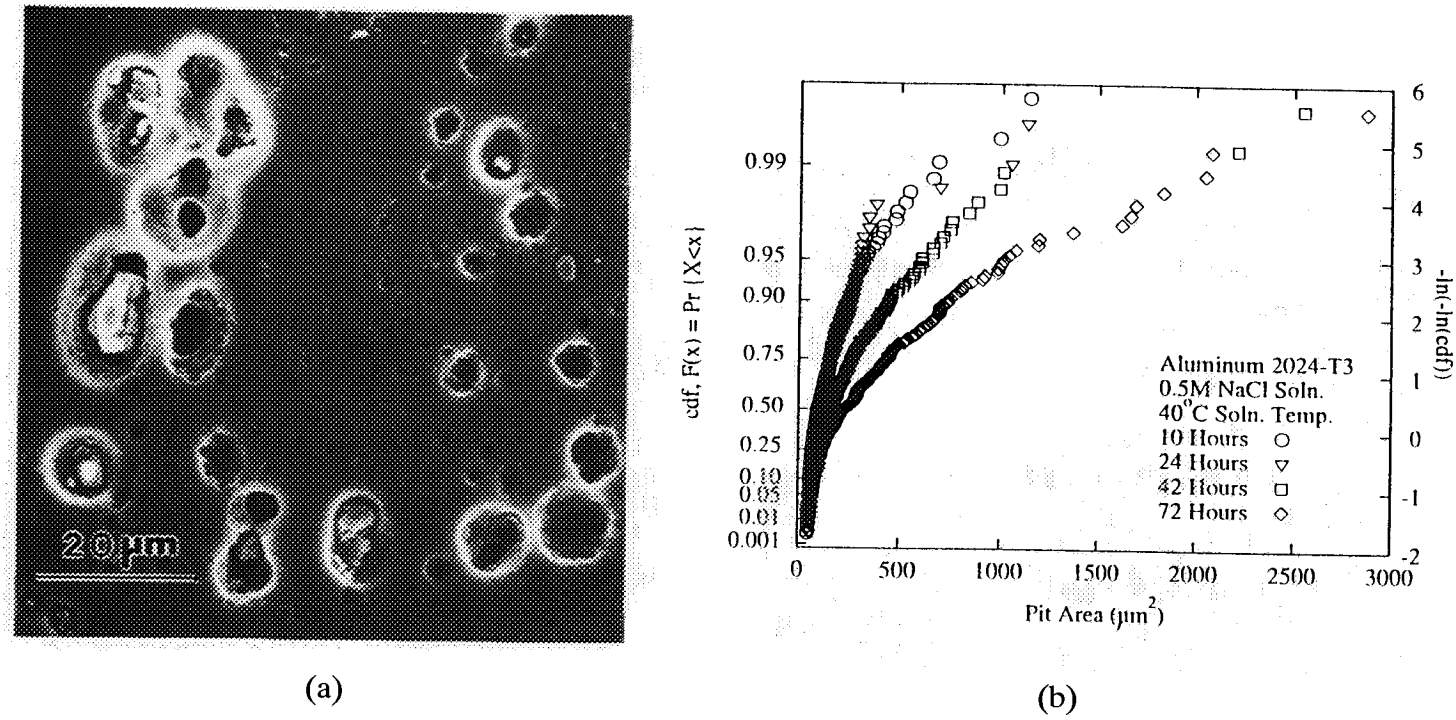

(a) (b)

Figure 8. (a) Coalescence of individual pits taking place laterally and in depth at the specimen surface to form a larger pit, and (b) a Gumbel plot of pit size (projected area) distribution over different corrosion time showing the evolution of pitting damage.

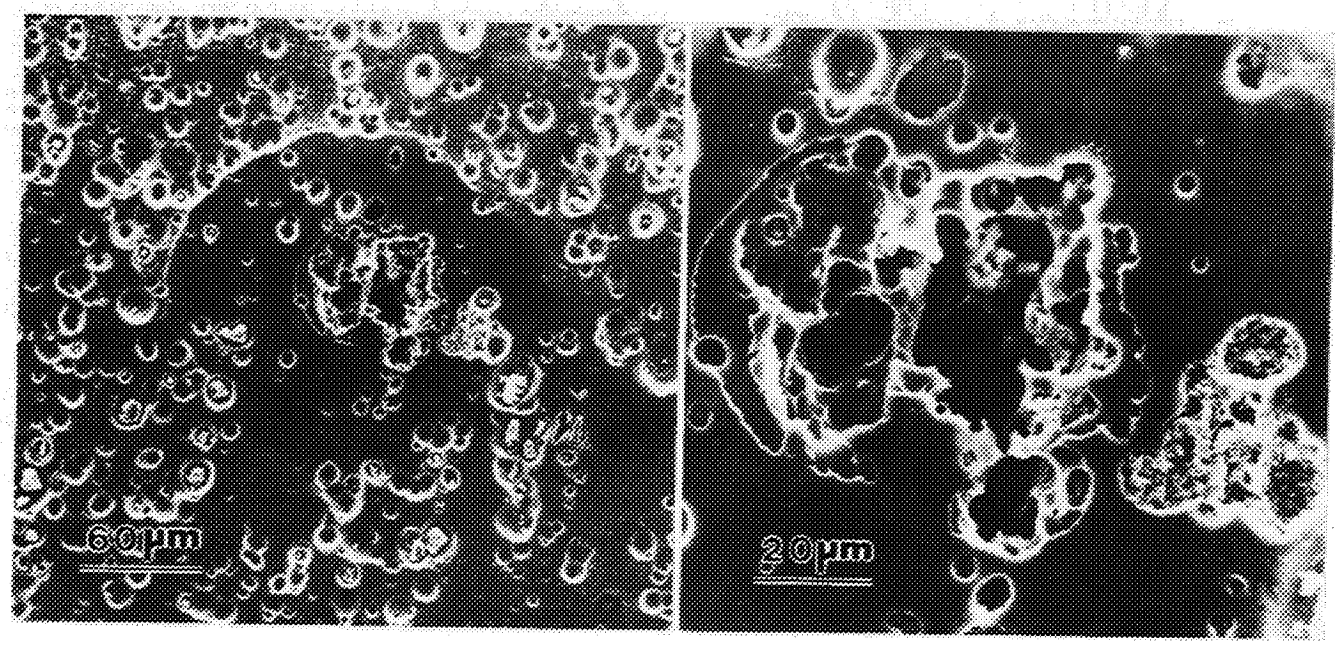

Figure 9. Corrosion features in the thickness orientation of a 2024-T3 aluminum specimen tested in 0.5M NaCl solution (pH = ~5.8) at room temperature for 3 days.

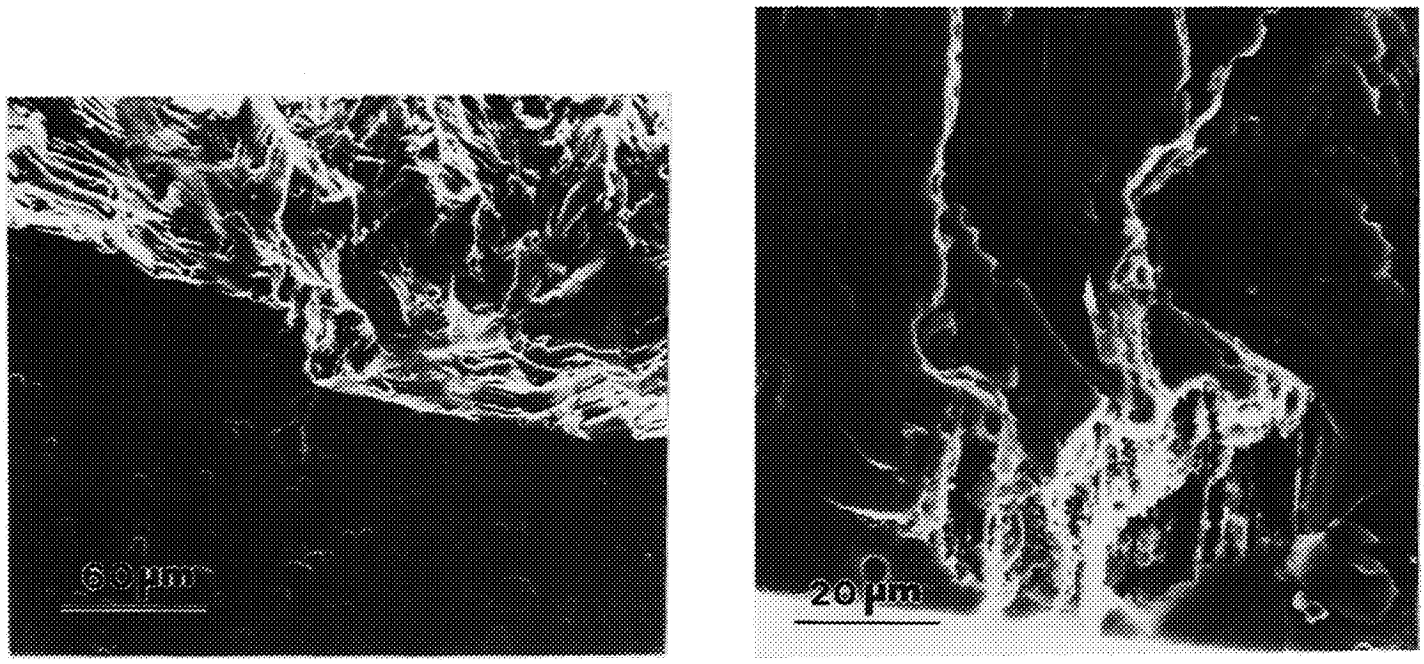

(a)

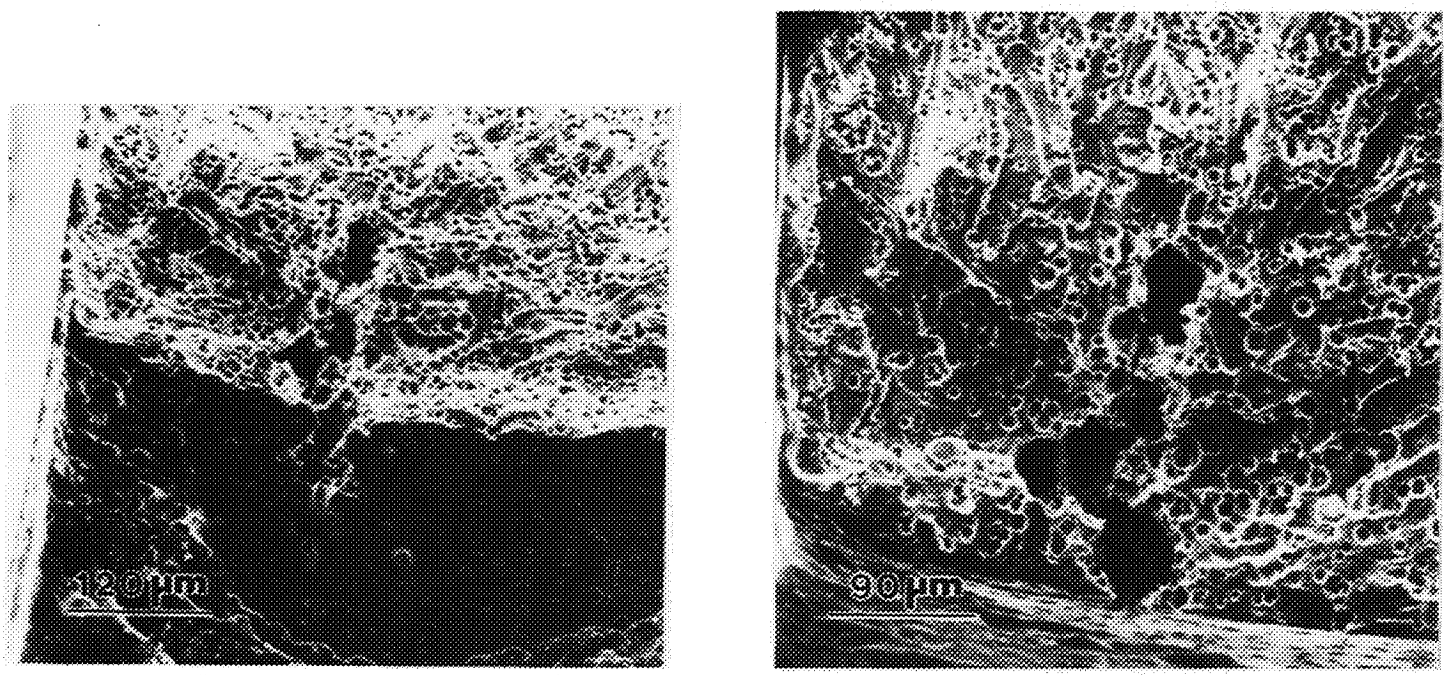

(b)

Figure 10. Corrosion fatigue crack nucleation associated with pits in 2024-T3 aluminum specimens tested in 0.5M NaCl solution at room temperature with σ_{max} = 320 MPa (R = 0.1); (a) f = 10 Hz, and (b) f = 0.1 Hz.

reflected *competition* between pitting corrosion and early corrosion fatigue crack growth. The addition of a growth rate requirement to the transition criterion, therefore, is needed; namely,

$$\Delta K \geq \Delta K_{th}$$

$$(da/dt)_{crack} \geq (da/dt)_{pit}$$

where ΔK_{th} is the threshold for fatigue crack growth, and (da/dt) refers to the appropriate crack and pit growth rates.

The extent of post-crack-growth pitting of the fracture surface also depended on frequency, which reflected the duration of exposure of the fracture surface to the electrolyte. The presence of localized corrosion (pitting) on the fatigue fracture surfaces (see Fig. 10b) further confirmed the competition between localized corrosion and corrosion fatigue crack growth.

A MECHANISTICALLY BASED PROBABILITY APPROACH TO LIFE PREDICTION

It was recognized that a quantitative methodology for life prediction is needed to help define suitable inspection intervals and assess the durability and integrity of aircraft components and structures. To be effective, this methodology must provide statistically accurate estimates of response for conditions not included within the available experimental observations, and account for the influences of key external and internal variables. The external variables include applied stress, environmental chemistry, and temperature; and the internal variables, chemistry within a pit or at the crack tip material properties, initial defect size, etc. (see Fig. 3). The development of such a methodology requires mechanistic understanding and quantification of the processes for damage accumulation. In other words, a mechanistically based probability approach to life prediction (or durability assessment) is needed.

The feasibility and utility of this approach have been demonstrated. A dominant flaw probability model for pitting and corrosion fatigue was developed as an illustrative example [12]. This model was based on an original model proposed by Kondo [9] and Kondo and Wei [10] which assumed pitting corrosion to proceed at a constant volumetric rate. Transition from pit (hemispherical) to crack (semi-circular) was based on a matching of the stress intensity factor for an equivalent semi-circular crack against the fatigue crack growth threshold. A power-law model was used to represent subsequent fatigue crack growth. The elemental models were assumed to capture some of the key mechanistic features, and provide reasonable "predictions" of response. The overall model incorporated initial defect size, corrosion rate, fatigue crack growth rate coefficient, and fatigue crack growth threshold (ΔK_{th}) as random variables, and permitted examinations of the contribution of each of these variables to the distribution in life. This model has been modified to account for corrosion and fatigue from an open circular hole. The modification included a further transition from the pitting initiated semi-circular surface crack at an open-hole to a through-thickness crack. A typical result showing the influence of loading frequency is shown in Fig 12.

These models are reasonably consistent with the foregoing observations of localized pitting corrosion and the subsequent nucleation and growth of a corrosion fatigue crack from a dominant pit.

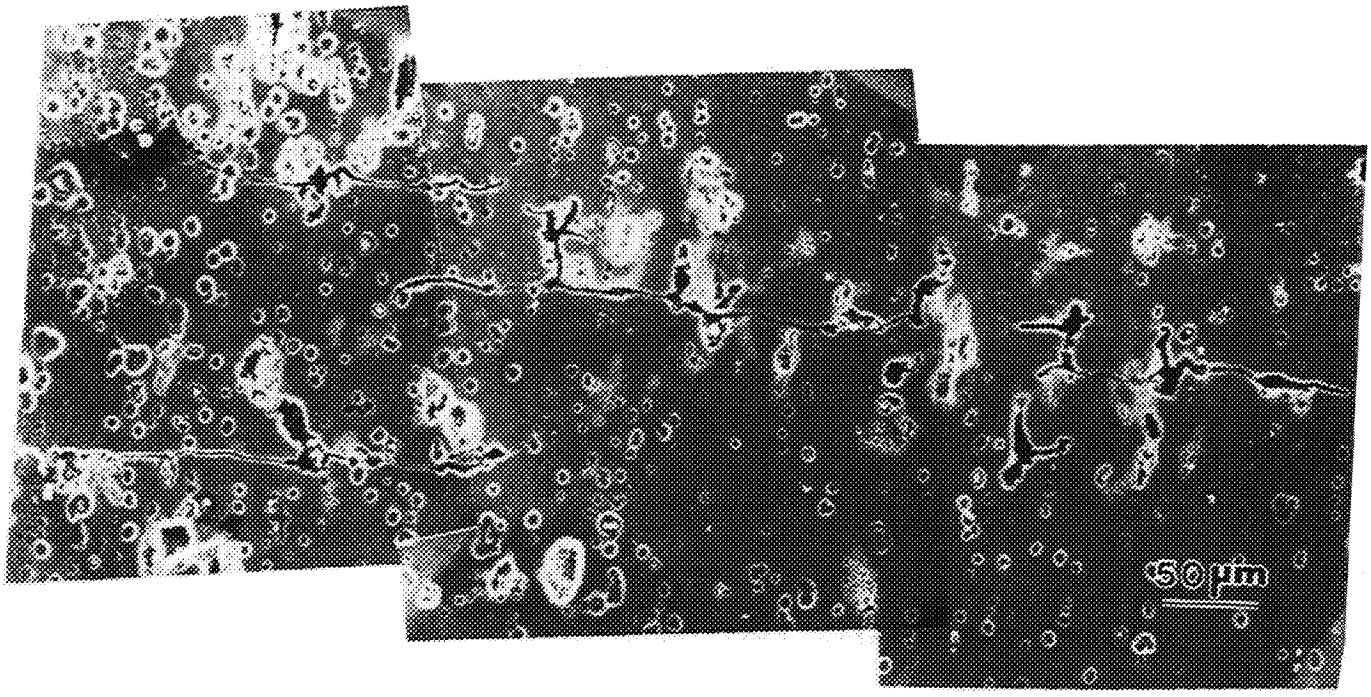

Figure 11. Secondary cracks forming (away from the main crack) at corrosion pits at the free surface of a fatigue specimen tested in 0.5M NaCl solution at room temperature with σ_{max} = 320 MPa (R = 0.1) and with f = 0.1 Hz.

Table III. Results for Corrosion Fatigue Crack Nucleation of the 2024-T3 Alloy in 0.5M NaCl Solution with σ_{max} = 320 MPa (R = 0.1) and with f = 0.1 to 20 Hz

Sample No.	Frequency [Hz]	N_i [cycles] / t_i [hrs]	N_f [cycles] / t_f [hrs]	(Pit Size)* $2c$ x a [µm]	(ΔK)** @ surface [MPa$\sqrt{m}$]
A01F29	20	*not available*	58,629 / 0.81	50 x 80	2.83
A01F14	10	29,700 / 0.83	78,745 / 2.19	45 x 35	2.27
A01F05	5	23,970 / 1.33	59,381 / 3.3	45 x 60	2.60
A01F39	5	27,470 / 1.53	64,800 / 3.6	40 x 60	2.50
A01F51	0.5	39,830 / 22.13	77,875 / 43.26	75 x 200	3.65
A01F08	0.5	41,138 / 22.85	*not available*	67 x 150	3.41
A01F20	0.1	18,635 / 51.76	57,809 / 160.58	100 x 250	4.20
A01F36†	5	8,000 / 0.44	67,392 / 3.74	100 x 150	3.96

† Three day pre-exposure to NaCl solution prior to corrosion fatigue testing.
* $2c$ = maximum width of the pit; a = maximum depth of the pit.
** See ref. [11] for the K estimation for a semi-elliptical surface crack.

The simplified concept of a single pit, however, would require more careful study. A more appropriate model will need to be developed to better represent the three dimensional nature of particle-induced pit nucleation, and their coalescence and growth in breadth and depth into a large pit. The kinetics and probabilistic aspects of pit growth would also require further attention, and are under investigation. In contrast to the simplifying assumption, fatigue crack nucleation from a corrosion pit (or the transition from pit to fatigue crack growth) was found to be dependent on the loading frequency. Additional efforts are underway to better characterize this frequency dependence and the kinetics of fatigue crack growth, and to incorporate them into the life prediction methodology.

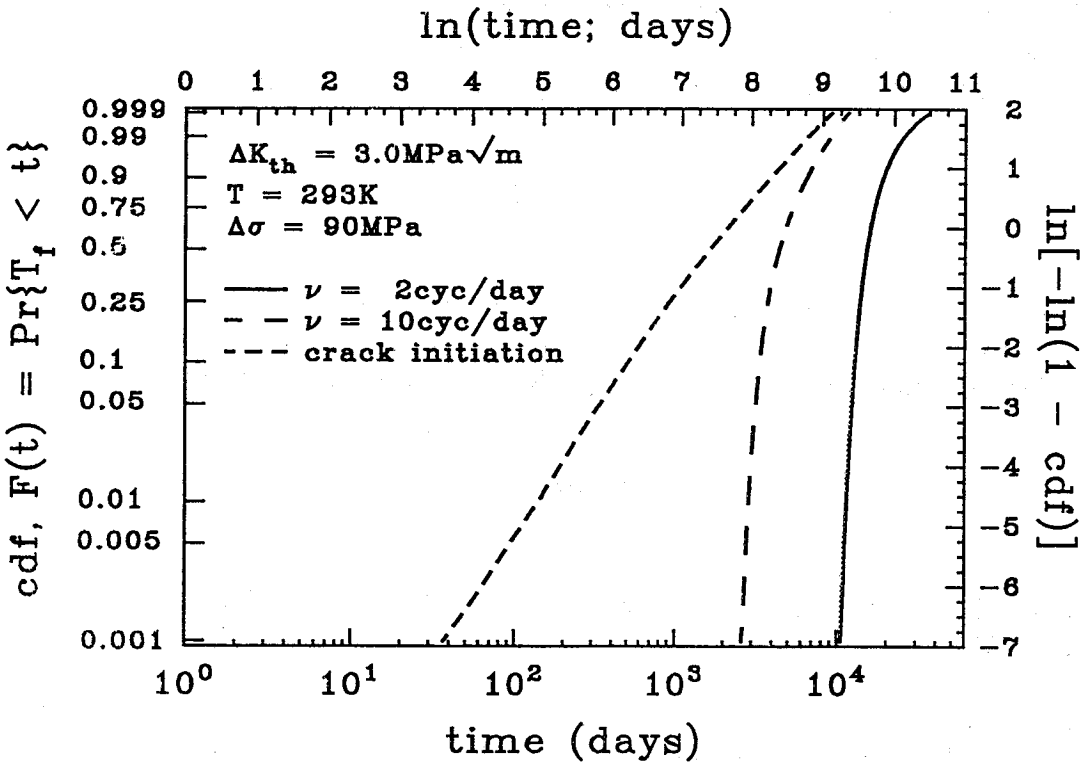

Figure 12. Relative contribution of the time-to-initiation and time-of-crack growth on the *cdf* for the time-to-failure at 293*K* and 90 MPa.

SUMMARY

The results show that bare 2024-T3 alloys corrode readily in 0.5M NaCl solution. The corrosion is promoted by the presence of constituent particles. The alloy used in this study contained over 3,000 constituent particles per square millimeter with projected area greater than 1 μm^2. Two types of particles were identified: one containing Al, Cu and Mg, and the other, Al, Cu, Mn and Fe. The Al-Cu-Mn-Fe-containing particles acted as cathodes and resulted in localized dissolution of the surrounding matrix, whereas the Al-Cu-Mg-containing particles acted as anodes and themselves dissolved.

The interactions between the particles, and between the particles and the matrix, result in the nucleation of pits. The growth and coalescence of pits, in depth and in breadth, led to the formation of large corrosion pits, from which corrosion fatigue cracks nucleate. The transition from pit to corrosion fatigue crack growth is determined not only by the need to overcome the threshold K value for fatigue crack growth, but also by the competition between pit and fatigue crack growth rates.

The particle-particle and particle-matrix interactions are complex, and need to be understood as a part of the program in developing models for corrosion damage evolution. A part of the complexity arises from clustering and banding of the particles along the rolling direction, which appear to be more severe in the thickness (S-L and S-T) orientations. The 3-dimensional nature of particle distribution and its influence on the growth of pits in depth as well as in breadth will need to be taken into account. This effort on corrosion and corrosion fatigue crack nucleation, along with studies of corrosion fatigue crack growth, are being continued to provide a mechanistic basis for life prediction.

ACKNOWLEDGMENTS

This research was supported by the Aging Airplane Program of the Federal Aviation Administration under Grant No. 92-G-0006, with Dr. Thomas H. Flournoy as Program Director. Assistance by Dr. Shuchun Chen and Mr. Joseph K.-C. Wan is gratefully acknowledged.

REFERENCES

1. Harlow, D. G.: The Effect of Proof-Testing on the Weibull Distribution. *J. Mater. Sci.*, vol. 24, 1989, p. 1467.

2. Buchheit, R. G. Jr.; Moran, J. P.; and Stoner, G. E.: Localized Corrosion Behavior of Alloy 2090 - The Role of Microstructural Heterogeneity. *Corrosion,* vol. 46, 1990, p. 610.

3. Sury, P.; and Oswald, H. R.: On the Corrosion Behavior of Individual Phases Present in Aluminum Bronzes. *Corrosion Sci.*, vol. 12, 1972, p. 77.

4. Hatch, J. E., ed.: *Aluminum: Properties and Physical Metallurgy.* ASM, Metals Park, OH, 1984, p. 259.

5. Murray, G. A. W.; Lamb, H. J.; and Godard, H. P.: Role of Iron in Aluminum on the Initiation of Pitting in Water. *Br. Corros. J.*, vol. 2, 1967, p. 216.

6. Bury, K. V.: *Statistical Models in Applied Science.* John Wiley & Sons, Inc., NY, 1975, p. 367.

7. Hoeppner, D. W.: Model for Prediction of Fatigue Lives Based upon a Pitting Corrosion Fatigue Process. *Fatigue Mechanisms.* STP 675, Fong, J. T., ed., ASTM, Philadelphia, PA, 1979, p. 841.

8. Muller, M.: Theoretical Considerations on Corrosion Fatigue Crack Initiation. *Met. Trans.*, vol. 13A, 1982, p. 649.

9. Kondo, Y.: Prediction of Fatigue Crack Initiation Life Based on Pit Growth. *Corrosion,* vol. 45, 1989, p. 7.

10. Kondo, Y.; and Wei, R. P.: Approach on Quantitative Evaluation of Corrosion Fatigue Initiation Condition. *Evaluation of Materials Performance in Severe Environments.* Proceedings of International Conference, The Iron and Steel Institute of Japan, Tokyo, Japan, 1989, p. 135.

11. Irwin, G. R.: Crack-Extension Force for A Part-Through Crack in A Plate. *J. Applied Mech. (Trans. ASME)*, December, 1962, p. 651.

12. Wei, R. P.; and Harlow, D. G.: A Mechanistically Based Probability Approach for Predicting Corrosion and Corrosion Fatigue Life. *Durability and Structural Integrity of Airframes.* Blom, A. F. ed., Engineering Materials Advisory Services Ltd., West Midlands, U. K., 1993, p. 347.